

Osman Turan
School of Engineering,
University of Liverpool,
Brownlow Hill,
Liverpool, L69 3GH, UK;
Department of Mechanical Engineering,
Karadeniz Technical University,
Trabzon, 61080, Turkey
e-mail: osmanturan@ktu.edu.tr

Anuj Sachdeva
e-mail: a.sachdeva@liv.ac.uk

Robert J. Poole
e-mail: robpoole@liv.ac.uk

School of Engineering,
University of Liverpool,
Brownlow Hill,
Liverpool, L69 3GH, UK

Nilanjan Chakraborty¹
School of Mechanical and Systems Engineering,
Newcastle University,
Claremont Road,
Newcastle-Upon-Tyne, NE1 7RU, UK
e-mail: nilanjan.chakraborty@ncl.ac.uk

Laminar Natural Convection of Power-Law Fluids in a Square Enclosure With Differentially Heated Sidewalls Subjected to Constant Wall Heat Flux

Two-dimensional steady-state laminar natural convection of inelastic power-law non-Newtonian fluids in square enclosures with differentially heated sidewalls subjected to constant wall heat flux (CHWF) are studied numerically. To complement the simulations, a scaling analysis is also performed to elucidate the anticipated effects of Rayleigh number (Ra), Prandtl number (Pr) and power-law index (n) on the Nusselt number. The effects of n in the range $0.6 \leq n \leq 1.8$ on heat and momentum transport are investigated for nominal values Ra in the range 10^3 – 10^6 and a Pr range of 10 – 10^5 . In addition the results are compared with the constant wall temperature (CWT) configuration. It is found that the mean Nusselt number \overline{Nu} increases with increasing values of Ra for both Newtonian and power-law fluids in both configurations. However, the \overline{Nu} values for the vertical walls subjected to CHWF are smaller than the corresponding values in the same configuration with CWT (for identical values of nominal Ra , Pr and n). The \overline{Nu} values obtained for power-law fluids with $n < 1$ ($n > 1$) are greater (smaller) than that obtained in the case of Newtonian fluids with the same nominal value of Ra due to strengthening (weakening) of convective transport. With increasing shear-thickening (i.e., $n > 1$) the mean Nusselt number \overline{Nu} settles to unity ($\overline{Nu} = 1.0$) as heat transfer takes place principally due to thermal conduction. The effects of Pr are shown to be essentially negligible in the range 10 – 10^5 . New correlations are proposed for the mean Nusselt number \overline{Nu} for both Newtonian and power-law fluids. [DOI: 10.1115/1.4007123]

Keywords: natural convection, power-law fluid, Nusselt number, Rayleigh number, Prandtl number

1 Introduction

Natural convection in rectangular enclosures with differentially heated vertical sidewalls is one of the most extensively analyzed configurations because of its fundamental importance as a “benchmark” geometry to study convection effects (and compare numerical techniques). Additionally the geometry has relevance to solar collectors, food preservation, compact heat exchangers, and electronic cooling systems among other practical applications. A large body of existing literature [1–3] is available for this configuration especially in the case of Newtonian fluids and an extensive review can be obtained in Ref. [4]. Relatively limited effort has been directed to the analysis of natural convection of non-Newtonian fluids in rectangular enclosures. The Rayleigh–Bénard configuration [5], which involves a rectangular enclosure with adiabatic vertical walls and differentially heated horizontal walls with the bottom wall at higher temperature, has been investigated for a range of different non-Newtonian models, including inelastic generalized Newtonian fluids (GNF) [6–9], fluids with a yield stress [10–12], and viscoelastic fluids [13].

Kim et al. [14] studied transient natural convection of non-Newtonian power-law fluids (power-law index $n \leq 1$) in a square enclosure with differentially heated vertical sidewalls subjected to constant wall temperatures (CWT). According to this study, the mean Nusselt number \overline{Nu} increases with decreasing power-law

index n for a given set of values of Rayleigh (Ra) and Prandtl (Pr) numbers. This result is consistent with the numerical findings of Ohta et al. [8] where the Sutterby model was used for analyzing transient natural convection of shear-thinning fluids in the Rayleigh–Bénard configuration. The strengthening of natural convection in rectangular enclosures for shear-thinning fluids was also confirmed by both experimental and numerical studies on microemulsion slurries by Inaba et al. [9] in the Rayleigh–Bénard configuration. Lamsaadi et al. [15,16] studied the effects of the power-law index on natural convection in the high Pr limit for both tall [15] and shallow enclosures [16] where the vertical sidewall boundary conditions are constant wall heat fluxes (CHWF) rather than isothermal vertical sidewalls as in Ref. [14]. Lamsaadi et al. [15,16] demonstrated that the convective heat transfer rate depends only on the values of nominal Ra and the power-law index n for large values of aspect ratio and the nominal Pr .² Barth and Carey [17] utilized GNF models that incorporate limiting viscosities at low and high shear rates to study a three-dimensional version of the problem (the adiabatic boundary conditions are replaced by a linear variation in temperature to match the experimental conditions of [18]). Vola et al. [19] and Turan et al. [20–22] numerically studied steady two-dimensional natural convection of yield stress fluids obeying the Bingham model in rectangular enclosures with vertical sidewalls subjected to both CWT [20,21] and CHWF [22]. Recently the present authors [23] carried out a numerical study for steady natural convection of power-law

¹Corresponding author.

Contributed by Heat Transfer Division of ASME for publication in the JOURNAL OF HEAT TRANSFER. Manuscript received July 24, 2011; final manuscript received April 3, 2012; published online October 8, 2012. Assoc. Editor: Sujoy Kumar Saha.

²The definitions of Ra and Pr are provided later in Sec. 2.

fluids in a square enclosure with differentially heated sidewalls subjected to CWT for the power-law index n range $0.6 \leq n \leq 1.8$, $Ra = 10^3 - 10^6$ and $Pr = 10 - 10^5$. A correlation has also been proposed for the mean Nusselt number \overline{Nu} based on the simulation data guided by a scaling analysis [23].

The present study extends the analysis of Turan et al. [23] by modifying the vertical sidewall boundary condition to the CWHF rather than CWT. The difference in heat transfer behavior of power-law fluids in a square enclosure due to a change in sidewall boundary condition (between CWT and CWHF) is yet to be addressed in the open literature. In this respect the main objectives of the present study are as follows:

- (1) to demonstrate the effects of n , Ra , and Pr on the mean Nusselt number \overline{Nu} in the case of natural convection of power-law fluids in a square enclosure with differentially heated vertical sidewalls subjected to CWHF
- (2) to identify the differences in the heat transfer behavior between the configurations with CWHF and CWT for the same values of Ra , Pr , and n
- (3) to develop a correlation for the mean Nusselt number for natural convection of power-law fluids in a square enclosure with differentially heated vertical sidewalls subjected to CWHF

The necessary mathematical background and numerical details will be presented in Sec. 2, which will be followed by the scaling analysis. Following this analysis, the results will be presented and subsequently discussed. The main findings will be summarized and conclusions will be drawn in Sec. 5.

2 Mathematical Background and Numerical Implementation

2.1 Governing Equations and Nondimensional Numbers.

For the present study steady-state flow of an incompressible power-law fluid is considered. For incompressible fluids the conservation equations for mass, momentum, and energy under steady state can be written using tensor notation (i.e., $x_1 = x$ is the horizontal direction and $x_2 = y$ is the vertical direction) as

- Mass conservation equation

$$\frac{\partial u_i}{\partial x_i} = 0 \quad (1)$$

- Momentum conservation equations

$$\rho u_j \frac{\partial u_i}{\partial x_j} = -\frac{\partial P}{\partial x_i} + \rho g \beta \delta_{i2} (T - T_{\text{ref}}) + \frac{\partial \tau_{ij}}{\partial x_j} \quad (2)$$

- Energy conservation equation

$$\rho u_j c_p \frac{\partial T}{\partial x_j} = \frac{\partial}{\partial x_j} \left(k \frac{\partial T}{\partial x_j} \right) \quad (3)$$

where for the CWHF configuration the reference temperature T_{ref} is taken to be the temperature at the geometrical center of the domain (i.e., $T_{\text{ref}} = T_{\text{cen}}$) for evaluating the buoyancy term $\rho g \beta \delta_{i2} (T - T_{\text{ref}})$ in the momentum conservation equations for the CWHF configuration (In contrast, T_{ref} is taken to be the cold wall temperature T_C for the CWT configuration [23]). The Kronecker δ_{i2} ensures that the buoyancy term $\rho g \beta \delta_{i2} (T - T_{\text{ref}})$ remains operational only in the momentum equation for the vertical direction (i.e., x_2 -direction). According to the Ostwald-De Waele (i.e., power law) model the viscous stress tensor τ_{ij} is given by

$$\tau_{ij} = \mu_a e_{ij} = K (e_{kl} e_{kl} / 2)^{(n-1)/2} e_{ij} \quad (4)$$

where $e_{ij} = (\partial u_i / \partial x_j + \partial u_j / \partial x_i)$ ($e_{kl} = (\partial u_k / \partial x_l + \partial u_l / \partial x_k)$) is a component of the rate of strain tensor, K is the consistency, n is the power-law index and μ_a is the apparent viscosity, which is given by

$$\mu_a = K (e_{kl} e_{kl} / 2)^{(n-1)/2} \quad (5)$$

For $n < 1$ ($n > 1$) the apparent viscosity decreases (increases) with increasing shear rate, and thus, the fluids with $n < 1$ ($n > 1$) are referred to as shear-thinning (shear-thickening) fluids. In the present study, natural convection of power-law fluids in a square enclosure (of dimension L) with differentially heated sidewalls is analyzed for different values of n and the nominal values of Ra and Pr for both CWT and CWHF boundary conditions.

The Rayleigh number Ra represents the ratio of the strengths of thermal transports due to buoyancy to thermal conduction, which can be defined in the following manner for CWHF boundary condition:

$$Ra_{\text{CWHF}} = \frac{\rho^2 c_p g \beta q L^4}{\mu_{\text{ref}} k^2} = Gr_{\text{CWHF}} Pr \quad (6)$$

where Gr_{CWHF} is the Grashof number in the CWHF condition and Pr is the Prandtl number, which are defined as

$$Gr_{\text{CWHF}} = \frac{\rho^2 g \beta q L^4}{\mu_{\text{ref}}^2 k} \quad \text{and} \quad Pr = \frac{\mu_{\text{ref}} c_p}{k} \quad (7)$$

For the CWT configuration the Ra and Grashof (Gr) numbers are defined as

$$Ra_{\text{CWT}} = \frac{\rho^2 c_p g \beta (T_H - T_C) L^3}{\mu_{\text{ref}} k} = Gr_{\text{CWT}} Pr \quad \text{and} \quad (8)$$

$$Gr_{\text{CWT}} = \frac{\rho^2 g \beta (T_H - T_C) L^3}{\mu_{\text{ref}}^2}$$

Gr represents the ratio of the strengths of the buoyancy and viscous forces while Pr depicts the ratio of the strengths of momentum diffusion to thermal diffusion. Alternatively, Pr can be taken to represent the ratio of the viscous boundary-layer to thermal boundary-layer thicknesses.

For power-law fluids—because the viscosity varies with the flow—in Eqs. (3)–(5) μ_{ref} represents the value of “reference” viscosity. An important consideration in heat and fluid flow problems for power-law fluids lies in the most appropriate choice of this nominal viscosity. The reference viscosity μ_{ref} can be defined based on a characteristic shear rate $\dot{\gamma}$, which can itself be scaled as $\dot{\gamma} \sim u_{\text{scale}} / L$ where u_{scale} is a velocity scale based on which μ_{ref} is estimated. Using a velocity scale given by $u_{\text{scale}} \sim \alpha / L$ as in Refs. [15,16,24], one can obtain the following expression for μ_{ref} :

$$\mu_{\text{ref}} \sim K \dot{\gamma}^{n-1} \sim K \left(\frac{\alpha}{L} \right)^{n-1} \quad (9)$$

Equation (9) only presents a representative value, which was used for analyzing natural convection in rectangular enclosures in several previous studies [15,16,24]. As the local shear rate $\dot{\gamma}$ cannot be a priori predicted, a velocity scale $u_{\text{scale}} \sim \alpha / L$ allows for expressing Ra , Gr , and Pr as functions of known quantities (i.e., $g, \beta, K, \rho, \alpha, k$ and L). Equations (6)–(8) give rise to the following definitions of Ra , Gr , and Pr :

$$Ra_{\text{CWHF}} = \frac{g \beta q L^{2n+2}}{(K/\rho) \alpha^n k}; \quad (10i)$$

$$Gr_{\text{CWHF}} = \frac{g \beta q L^{4n}}{(K/\rho)^2 \alpha^{2n-2} k} \quad \text{and} \quad Pr = \left(\frac{K}{\rho} \right) \alpha^{n-2} L^{2-2n}$$

$$\begin{aligned} \text{Ra}_{\text{CWT}} &= \frac{g\beta(T_H - T_C)L^{2n+1}}{\alpha^n(K/\rho)}; \\ \text{Gr}_{\text{CWT}} &= \frac{g\beta(T_H - T_C)L^{4n-1}}{(K/\rho)^2\alpha^{2n-2}}; \text{ and } \text{Pr} = \left(\frac{K}{\rho}\right)\alpha^{n-2}L^{2-2n} \end{aligned} \quad (10ii)$$

These definitions, which will be used for the remainder of this paper, are the same as those used by Ng and Hartnett [24] and Lamsaadi et al. [15,16]. It might be more appropriate to use a velocity scale based on buoyancy effects (i.e., $u_{\text{scale}} \sim \sqrt{g\beta q L^2/k}$ for CWHF and $u_{\text{scale}} \sim \sqrt{g\beta(T_H - T_C)L}$ for CWT) to define the reference viscosity as $\bar{\mu}_{\text{ref}} \sim K(\sqrt{g\beta q/k})^{n-1}$ and $\bar{\mu}_{\text{ref}} \sim K(\sqrt{g\beta(T_H - T_C)L})^{n-1}$ for CWHF and CWT boundary conditions, respectively, which will yield the following alternative expressions of Ra, Gr, and Pr:

$$\begin{aligned} \bar{\text{Ra}}_{\text{CWHF}} &= \frac{(g\beta q/k)^{(3-n)/2}L^4}{\alpha(K/\rho)}; \quad \bar{\text{Gr}}_{\text{CWHF}} = \frac{(g\beta q/k)^{2-n}L^4}{(K/\rho)^2}; \quad \text{and} \\ \bar{\text{Pr}}_{\text{CWHF}} &= \left(\frac{K}{\rho}\right)\frac{(g\beta q/k)^{(n-1)/2}}{\alpha} \end{aligned} \quad (10iii)$$

$$\begin{aligned} \bar{\text{Ra}}_{\text{CWT}} &= \frac{[g\beta(T_H - T_C)]^{(3-n)/2}L^{(5+n)/2}}{(K/\rho)\alpha}; \\ \bar{\text{Gr}}_{\text{CWT}} &= \frac{[g\beta(T_H - T_C)]^{(2-n)}L^{2+n}}{(K/\rho)^2}; \quad \text{and} \\ \bar{\text{Pr}}_{\text{CWT}} &= \left(\frac{K}{\rho}\right)\frac{[g\beta(T_H - T_C)/L]^{(n-1)/2}}{\alpha} \end{aligned} \quad (10iv)$$

Ra, Gr, and Pr given by Eq. (10iii) (Eq. (10iv)) are related to Ra_{CWHF} , Gr_{CWHF} , and Pr (Ra_{CWT} , Gr_{CWT} , and Pr) in the following manner:

$$\begin{aligned} \bar{\text{Ra}}_{\text{CWHF}} &= \text{Ra}_{\text{CWHF}}^{(3-n)/2} \text{Pr}^{(1-n)/2}; \quad \bar{\text{Gr}}_{\text{CWHF}} = \text{Gr}_{\text{CWHF}}^{2-n} \text{Pr}^{-2(n-1)}; \quad \text{and} \\ \bar{\text{Pr}}_{\text{CWHF}} &= \text{Pr}^{(n+1)/2} \text{Ra}_{\text{CWHF}}^{(n-1)/2} \\ \bar{\text{Ra}}_{\text{CWT}} &= \text{Ra}_{\text{CWT}}^{(3-n)/2} \text{Pr}^{(1-n)/2}; \quad \bar{\text{Gr}}_{\text{CWT}} = \text{Gr}_{\text{CWT}}^{2-n} \text{Pr}^{-2(n-1)}; \quad \text{and} \\ \bar{\text{Pr}}_{\text{CWT}} &= \text{Pr}^{(n+1)/2} \text{Ra}_{\text{CWT}}^{(n-1)/2} \end{aligned} \quad (10v)$$

It is clear from Eq. (10v) (Eq. (10vi)) that Ra_{CWHF} , Gr_{CWHF} , and Pr (Ra_{CWT} , Gr_{CWT} , and Pr) are closely related to $\bar{\text{Ra}}_{\text{CWHF}}$, $\bar{\text{Gr}}_{\text{CWHF}}$, and $\bar{\text{Pr}}_{\text{CWHF}}$ ($\bar{\text{Ra}}_{\text{CWT}}$, $\bar{\text{Gr}}_{\text{CWT}}$, and $\bar{\text{Pr}}_{\text{CWT}}$). Moreover, Ra_{CWHF} , Gr_{CWHF} , and Pr (Ra_{CWT} , Gr_{CWT} , and Pr) become exactly equal to $\bar{\text{Ra}}_{\text{CWHF}}$, $\bar{\text{Gr}}_{\text{CWHF}}$, and $\bar{\text{Pr}}_{\text{CWHF}}$ ($\bar{\text{Ra}}_{\text{CWT}}$, $\bar{\text{Gr}}_{\text{CWT}}$, and $\bar{\text{Pr}}_{\text{CWT}}$) for Newtonian fluids (i.e., $n = 1$). Here the expressions given by Eqs. (10i) and (10ii) will be used for the sake of avoiding confusion as these definitions were used previously by Ng and Hartnett [24] and Lamsaadi et al. [15,16] in their analysis of natural convection of power-law fluids in rectangular enclosures. However, there is no unique definition of reference viscosity in power-law fluids with $n \neq 1$ and the definitions presented in Eqs. (10iii) and (10iv) are equally valid and legitimate choices for definitions of nominal Ra, Gr, and Pr numbers. However, the definition of Pr according to Eqs. (10i) and (10ii) does not change with the change in boundary condition. This makes the choice of $u_{\text{scale}} \sim \alpha/L$ more convenient for the subsequent analysis. Henceforth, the definitions given by Eqs. (10i) and (10ii) will be used in this paper.

Using dimensional analysis it is possible to show that for natural convection of power-law fluids in square enclosures $\text{Nu} = f_1(\text{Ra}, \text{Pr}, n)$, where the Nusselt number Nu is given by

$$\text{Nu} = \frac{hL}{k} \quad (11)$$

where Nu represents the ratio of heat transfer rate by convection to that by conduction in the fluid in question and the local heat transfer coefficient h is defined as

$$h = \left| -k \frac{\partial T}{\partial x_1} \right|_{\text{wf}} \times \frac{1}{(T_{x_1=0} - T_{x_1=L})} = \left| \frac{q}{(T_{x_1=0} - T_{x_1=L})} \right| \quad (12)$$

where the subscript “wf” refers to the condition of the fluid in contact with the wall. It is worth noting that the wall temperatures $T_{x_1=0}$ and $T_{x_2=L}$ are not constant along the wall (i.e., $T_{x_1=0}$ and $T_{x_2=L}$ are functions of vertical coordinate) for the CWHF boundary condition and this will be demonstrated in Sec. 4 of this paper.

2.2 Numerical Implementation. A finite-volume code is used to solve the coupled conservation equations of mass, momentum, and energy. In this framework, a second-order central differencing is used for the diffusive terms and a second-order upwind scheme for the convective terms. Coupling of the pressure and velocity is achieved using the well-known SIMPLE (semi-implicit method for pressure-linked equations) algorithm [25]. The convergence criteria were set to 10^{-7} for all the relative (scaled) residuals.

2.3 Boundary Conditions and Mesh. The schematic diagrams of the simulation domains for both the CWT and CWHF configurations are shown in Fig. 1. Both velocity components (i.e., u_1 and u_2) are identically zero on each boundary because of the no-slip condition and impenetrability of rigid boundaries. The heat fluxes for the cold and hot vertical walls are specified (i.e., $k(\partial T/\partial x_1)|_{x_1=0} = q$ and $k(\partial T/\partial x_1)|_{x_1=L} = q$). The temperature boundary conditions for the horizontal insulated boundaries are given by: $\partial T/\partial x_2 = 0$ at $x_2 = 0$ and $x_2 = L$. Here four governing equations (1 continuity + 2 momentum + 1 energy) for four quantities (u , v , p , T) are solved, and thus, no further boundary conditions are needed for pressure. The mesh used corresponds to mesh M2 from Ref. [23]. The numerical uncertainty is also of the same order as the CWT results presented in Ref. [23] and so extensive details are not unnecessarily repeated here. Essentially the mean Nusselt number values reported here are accurate to within 1% for all cases.

3 Scaling Analysis

A scaling analysis is performed to elucidate the anticipated effects of Ra, Pr, and n on the Nusselt number for power-law fluids. All the unknown constants involved in this scaling analysis are considered to be unity for the purpose of mathematical manipulations. The wall heat flux q can be scaled as

$$q \sim k \frac{\Delta T}{\delta_{th}} \sim h \Delta T \quad (13)$$

which gives rise to the following relation:

$$\text{Nu} \sim \frac{hL}{k} \sim \frac{L}{\delta_{th}} \quad \text{or} \quad \text{Nu} \sim \frac{L}{\delta} f_2(\text{Ra}, \text{Pr}, n) \quad (14)$$

where the thermal boundary-layer thickness δ_{th} is related to the hydrodynamic boundary-layer thickness δ in the following manner: $\delta/\delta_{th} \sim f_2(\text{Ra}, \text{Pr}, n)$, where $f_2(\text{Ra}, \text{Pr}, n)$ is a function of

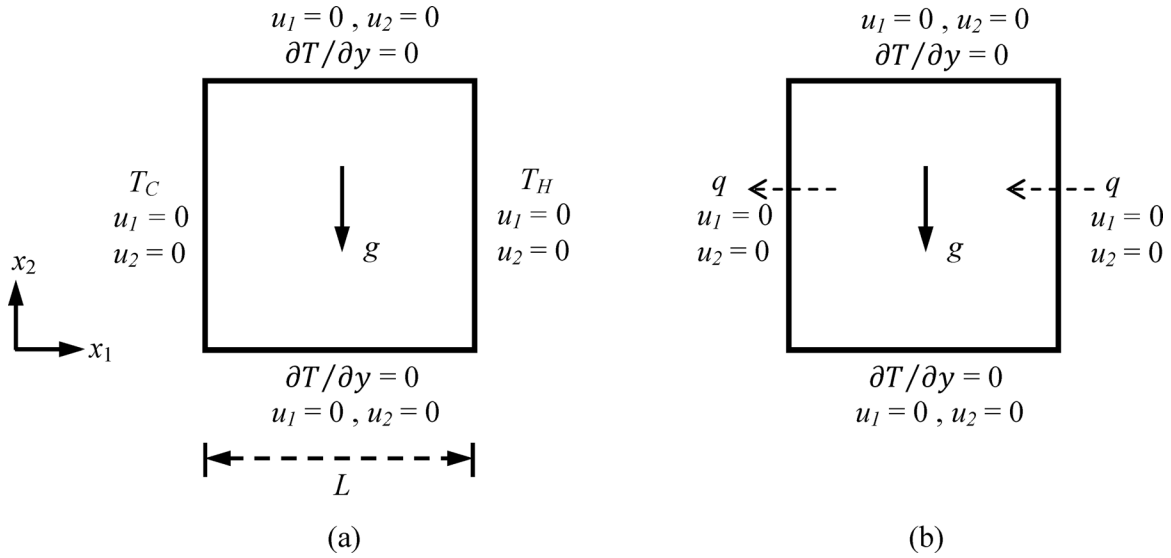


Fig. 1 Schematic diagram of the simulation domain (a) CWT configuration, (b) CWHF configuration

Rayleigh number, Prandtl number, and power-law index, which is expected to increase with increasing Pr. In order to estimate the thermal boundary-layer thickness δ_{th} , a balance of buoyancy and viscous forces in the vertical direction (i.e., x_2 -direction) is considered

$$\rho g \beta \Delta T \sim \rho g \beta q \delta_{th} / k \sim \frac{\tau}{\delta} \quad (15)$$

For power-law fluids the shear stress τ can be estimated as $\tau \sim K(\vartheta/\delta)^n$, where ϑ is a characteristic velocity scale, which upon substitution into Eq. (15) gives

$$\frac{\rho g \beta q \delta_{th}}{k} \sim K \frac{\vartheta^n}{\delta^{n+1}} \quad (16)$$

For natural convection the flow is induced by the buoyancy force, and thus, an equilibrium of inertial and buoyancy forces gives

$$\rho \frac{\vartheta^2}{L} \sim \rho g \beta \Delta T \sim \frac{\rho g \beta q \delta_{th}}{k} \quad (17)$$

This balance leads to an expression for the characteristic velocity scale

$$\vartheta \sim \sqrt{\frac{g \beta q \delta_{th} L}{k}} \quad (18)$$

which can be used in Eq. (16) to estimate the thermal boundary-layer thickness as

$$\delta_{th} \sim \left[\frac{K}{\rho} \left(\frac{g \beta q}{k} \right)^{n/2-1} \frac{L^{n/2}}{f_2^{n+1}} \right]^{\frac{1}{n/2+2}} \quad (19)$$

This scaling gives rise to the following expression for the thermal boundary-layer thickness δ_{th} :

$$\delta_{th} \sim \min \left[L, \frac{1}{f_2^{\frac{n+1}{n/2+2}}} \frac{L}{\left(\text{Ra}_{\text{CWHF}}^{1-n/2} \text{Pr}^{-n/2} \right)^{\frac{1}{n/2+2}}} \right] \sim \min \left[L, \frac{1}{f_3 (\text{Ra}_{\text{CWHF}}, \text{Pr}, n)} \frac{L}{\left(\text{Ra}_{\text{CWHF}}^{1-n/2} \text{Pr}^{-n/2} \right)^{\frac{1}{n/2+2}}} \right] \quad (20)$$

where Ra_{CWHF} and Pr are given by Eq. (10i) and f_3 is given by $f_3 = f_2^{(n+1)/(n/2+2)}$. The above expression accounts for the fact the thermal boundary-layer thickness becomes of the order of the enclosure size L under very high values of n when thermal conduction becomes the principal mode of heat transfer. Moreover, for a given set of values of Ra and Pr the thermal boundary-layer and hydrodynamic boundary-layer thicknesses (i.e., δ_{th} and δ) decrease with decreasing n . Equation (20) suggests that δ_{th} decreases with increasing Ra for $n < 2$. It is worth noting that Eq. (20) provides a representative thermal boundary layer thickness δ_{th} but in reality it varies along the wall. As δ_{th} is not a priori known, using a representative value of δ_{th} to obtain a reference viscosity μ_{ref} based on the characteristic shear rate ϑ/δ is unlikely to yield any extra benefit over the current methodology used for defining Ra, Gr, and Pr numbers (see Eq. (10i)).

Substitution of Eq. (20) into Eq. (13) yields

$$\overline{\text{Nu}} \sim \left(\text{Ra}_{\text{CWHF}}^{1-n/2} \text{Pr}^{-n/2} \right)^{\frac{1}{n/2+2}} f_3 (\text{Ra}_{\text{CWHF}}, \text{Pr}, n) \quad \text{when } \overline{\text{Nu}} > 1 \quad (21)$$

The mean Nusselt number $\overline{\text{Nu}}$ attains a value equal to unity (i.e., $\overline{\text{Nu}} = 1.0$) when δ_{th} approaches the enclosure size L . The scaling predictions provide useful insight into the anticipated behavior of $\overline{\text{Nu}}$ in response to variations of Ra, Pr, and n . Equation (21) suggests that $\overline{\text{Nu}}$ is expected to decrease with increasing n for a given value of Ra, whereas $\overline{\text{Nu}}$ increases with increasing Ra for a given value of n for $n < 2$. It is also important to note that the mean Nusselt number $\overline{\text{Nu}}$ behavior for Newtonian fluids can be obtained by setting $n = 1$ in Eq. (21).

An apparent effective viscosity μ_{eff} can be estimated in the following manner:

$$\mu_{eff} \sim K(\vartheta/\delta)^{n-1} \quad (22)$$

Using Eqs. (18) and (19) in Eq. (22) yields

$$\mu_{eff} \sim \rho \left(\frac{K}{\rho} \right)^{\frac{5}{n+4}} \left(\frac{g\beta q}{k} \right)^{(3n-3)/(n+4)} \times L^{(2n-2)/(n+4)} [f_2(\text{Ra}_{\text{CWHF}}, \text{Pr}, n)]^{\frac{2n^2+3n-5}{n+4}} \quad (23)$$

Equation (23) can be used to estimate effective Gr and Ra numbers (i.e., $\text{Gr}_{\text{CWHF,eff}}$ and $\text{Ra}_{\text{CWHF,eff}}$)

$$\text{Gr}_{\text{CWHF,eff}} = \frac{\rho^2 g \beta q L^4}{\mu_{eff}^2 k} \sim \text{Gr}_{\text{CWHF}}^{(10-5n)/(n+4)} \text{Pr}^{(10-10n)/(n+4)} \sim \text{Ra}_{\text{CWHF}}^{(10-5n)/(n+4)} \text{Pr}^{(-5n)/(n+4)} \quad (24)$$

$$\text{Ra}_{\text{CWHF,eff}} = \frac{\rho^2 c_p g \beta q L^4}{\mu_{eff} k^2} \frac{\mu_{eff} c_p}{k} \sim \text{Ra}_{\text{CWHF}}^{(7-2n)/(n+4)} \text{Pr}^{(2-2n)/(n+4)} \quad (25)$$

A similar scaling analysis has also been carried out for the CWT configuration by Turan et al. [23], which will be discussed later in Sec. 4.3 of this paper.

The relations given by Eqs. (24) and (25) indicate that the effective values of Gr and Ra become increasingly larger than their nominal values for decreasing values of n (especially for $n < 1$). This suggests that for small values of n the magnitudes of $\text{Gr}_{\text{CWHF,eff}}$ and $\text{Ra}_{\text{CWHF,eff}}$ may attain such values that a steady two-dimensional laminar solution may not exist, whereas a steady laminar solution can be obtained for the same set of nominal values of Ra_{CWHF} and Pr for a higher value of n . Thus, a critical value Ra_{crit} can be expected for the effective Rayleigh number $\text{Ra}_{\text{CWHF,eff}}$ such that a steady two-dimensional solution does not exist when $\text{Ra}_{\text{CWHF,eff}} > \text{Ra}_{\text{CWHF,crit}}$. A number of simulations have been carried out for different values of Ra_{CWHF} , Pr, and n and it has been found that a converged steady solution cannot be obtained when $\text{Ra}_{\text{CWHF,eff}} > 10^{5n+5} \text{Pr}^2$ (“unsteady” numerical solutions can be obtained, however) and the critical effective Ra above which a steady two-dimensional solution was not obtained can be given as

$$\text{Ra}_{\text{CWHF,crit}} \sim \text{Ra}_{\text{CWHF}}^{(7-2n)/(n+4)} \text{Pr}^{(2-2n)/(n+4)} = 10^{5n+5} \text{Pr}^2 \quad (26i)$$

which essentially suggests that steady two-dimensional solutions do not exist for the following condition:

$$\text{Ra}_{\text{CWHF}} > \left[10^{5n+5} \text{Pr}^{\frac{4n+6}{n+4}} \right]^{\frac{n+4}{7-2n}} \quad (26ii)$$

In contrast, the critical effective Ra above which a steady two-dimensional solution was not obtained in the case of CWT boundary condition can be summarized as follows [23]:

$$\text{Ra}_{\text{crit}} \sim \text{Ra}_{\text{CWT}}^{\frac{5-n}{2n+2}} \text{Pr}^{\frac{1-n}{2n+2}} = 10^7 \text{Pr} \quad (27)$$

Equation (27) suggests that steady two-dimensional solutions cannot be obtained for the following condition [23]:

$$\text{Ra}_{\text{CWT}} > \left[10^7 \text{Pr}^{\frac{3n+1}{2n+2}} \right]^{\frac{2n+2}{5-n}} \quad (28)$$

Moreover, a lower limit for Ra can be obtained using Eq. (21) above which convective transport plays a key role in heat transfer. For convective heat transfer to play an important role in the thermal transport, the mean Nusselt number $\overline{\text{Nu}}$ needs to exceed 1.0 (i.e., $\text{Nu} > 1$), and thus, the limiting condition for which convective heat transfer becomes important can be estimated as

$$\overline{\text{Nu}} \sim \left(\text{Ra}_{\text{CWHF}} \text{Pr}^{-n/2} \right)^{\frac{1}{n/2+2}} f_3(\text{Ra}_{\text{CWHF}}, \text{Pr}, n) \sim 1.0 \quad (29)$$

Considering $f_3(\text{Ra}_{\text{CWHF}}, \text{Pr}, n) \sim 1.0$ one obtains the following limiting condition:

$$\text{Ra}_{\text{CWHF}} \sim \text{Pr}^{\frac{n}{2-n}} \quad (30)$$

This condition is the same with the CWT configuration that has been recently studied by Turan et al. [23]. The conditions given by Eqs. (26)–(30) are shown in a regime diagram in Fig. 2(a). When $\text{Ra}_{\text{CWHF}} < \text{Pr}^{n/(2-n)}$ the heat transfer takes place principally due to thermal conduction, and therefore, this regime in Fig. 2(a) is referred to as the “conduction-dominated regime.” The region given by $[10^{5n+5} \text{Pr}^{(4n+6)/(n+4)}]^{(n+4)/(7-2n)} > \text{Ra}_{\text{CWHF}} > \text{Pr}^{n/(2-n)}$ in Fig. 2(a) is referred to as the “steady laminar convection regime” in the CWHF configuration. For the CWT configuration the steady laminar convection regime is given by $[10^7 \text{Pr}^{(3n+1)/(2n+2)}]^{(2n+2)/(5-n)} > \text{Ra}_{\text{CWT}} > \text{Pr}^{n/(2-n)}$ [23]. As steady two-dimensional laminar solutions do not exist for $\text{Ra}_{\text{CWHF}} > [10^{5n+5} \text{Pr}^{(4n+6)/(n+4)}]^{(n+4)/(7-2n)}$, the corresponding regime is referred to as the “unsteady convection regime” in the CWHF configuration, whereas the unsteady convection regime in the CWT configuration is characterized by $\text{Ra}_{\text{CWT}} > [10^7 \text{Pr}^{(3n+1)/(2n+2)}]^{(2n+2)/(5-n)}$ [23]. Figure 2 demonstrates that the boundaries of the conduction-dominated regime remain the same for both CWT and CWHF configurations, whereas the boundaries of the unsteady convection regime are quite different for the CWT and CWHF configurations. The validity of the above regime diagram can be substantiated from a series of unsteady calculations labeled cases A, B, C, and D and shown on the regime diagram. For cases A and B the mean Nusselt number $\overline{\text{Nu}}$ turns out to be steady for both CWT and CWHF configurations (i.e., case A: $\overline{\text{Nu}} = 1.0$), as predicted by the regime diagram. In case C a time-independent value of $\overline{\text{Nu}}$ is obtained for the CWHF configuration, whereas a complex transient behavior of $\overline{\text{Nu}}$ is obtained for the CWT configuration. The transient simulations for case D yielded a complex transient response of $\overline{\text{Nu}}$ for both CWT and CWHF configurations as observed from Fig. 2(b). It is important to note that the boundaries that distinguish one regime from another on the regime diagram shown in Fig. 2(a) are based on scaling arguments so these boundaries should not be treated rigidly but need to be considered only in an order of magnitude sense.

4 Results and Discussion

4.1 Effects of Power-Law Index n . The variations of nondimensional temperature $\theta = (T - T_{\text{cen}})k/qL$ and nondimensional vertical velocity component $V = u_2 L/\alpha$ along the horizontal mid-plane (i.e., $x_2/L = 0.5$) for $\text{Ra}_{\text{CWHF}} = 10^4, 10^5$, and 10^6 at $\text{Pr} = 10^4$ are shown in Figs. 3(a) and 3(b), respectively, for different values of n ranging from 0.6 to 1.8. Data for the other Pr cases studied ($10-10^5$) are virtually identical and are, therefore, not shown. For

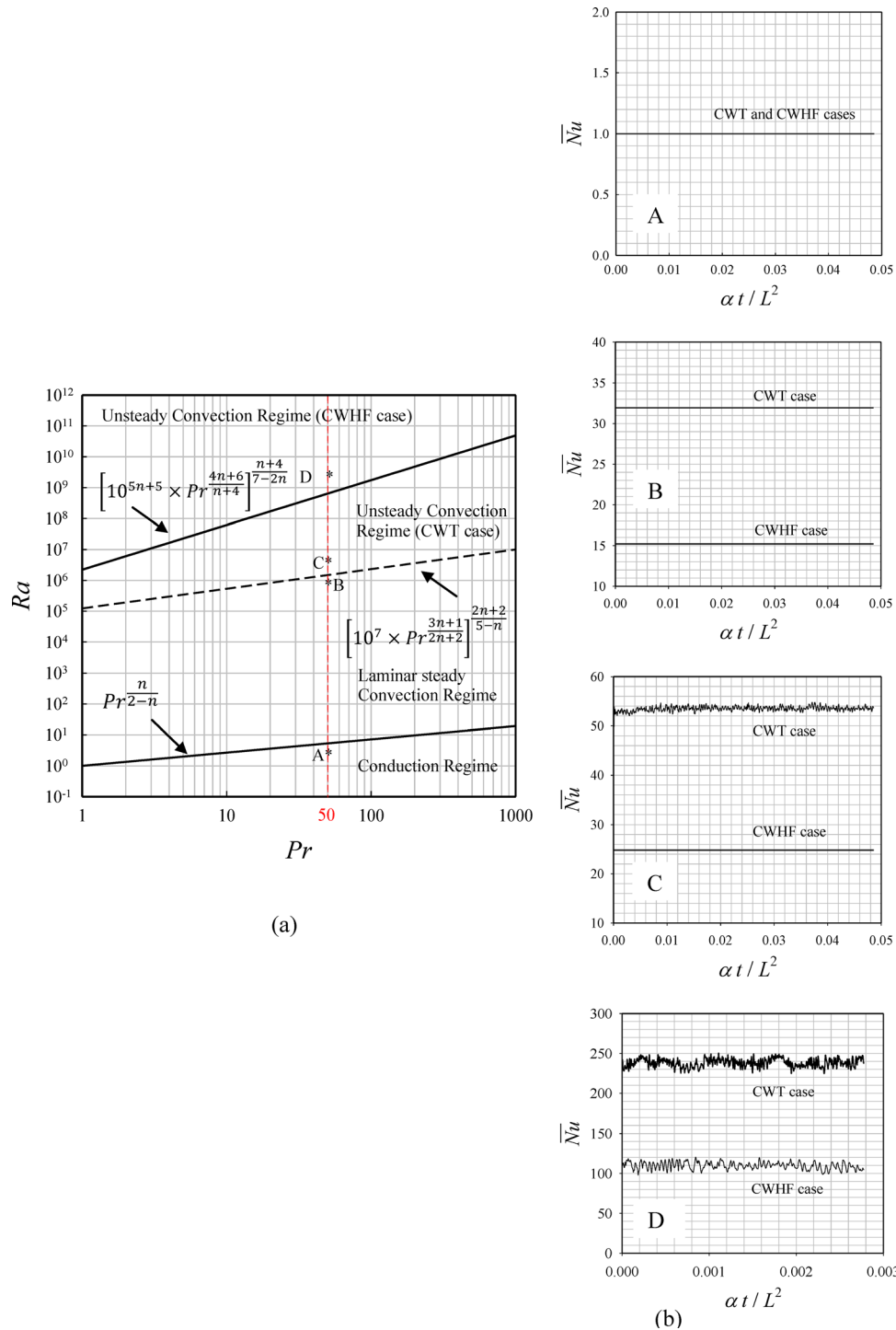


Fig. 2 (a) Different regimes of convection for both CWT and CWHF configurations for $n = 0.6$, (b) temporal evolution of \overline{Nu} with dimensionless time $\alpha t / L^2$ at $Pr = 50$, $n = 0.6$ for: (A) conduction regime Ra_{CWHF} (Ra_{CWT}) = 5, (B) laminar steady convection regime Ra_{CWHF} (Ra_{CWT}) = 1×10^6 , (C) CWT case unsteady convection regime Ra_{CWHF} (Ra_{CWT}) = 5×10^6 , (D) CWHF case unsteady convection regime Ra_{CWHF} (Ra_{CWT}) = 5×10^9

example, for the Newtonian and shear-thickening fluids the differences in mean Nusselt number for the different Pr cases are less than 0.1%. For the most shear-thinning fluid (i.e., $n = 0.6$) very minor differences due to Pr are observed but these correspond to increases in the mean Nusselt number of 0.35% ($Ra = 10^4$), 0.70% ($Ra = 10^5$), and 1.4% ($Ra = 10^6$). The distributions of

$U = u_1 L / \alpha$ are not separately shown here because U and V remain of the same order in a square enclosure according to continuity (i.e., $u_1 / L \sim u_2 / L$). It can be seen from Fig. 3 that, at a given Ra_{CWHF} , the variation of temperature exhibits increasing boundary layer character with decreasing values of n . This increasing trend of boundary layer character with decreasing values of n

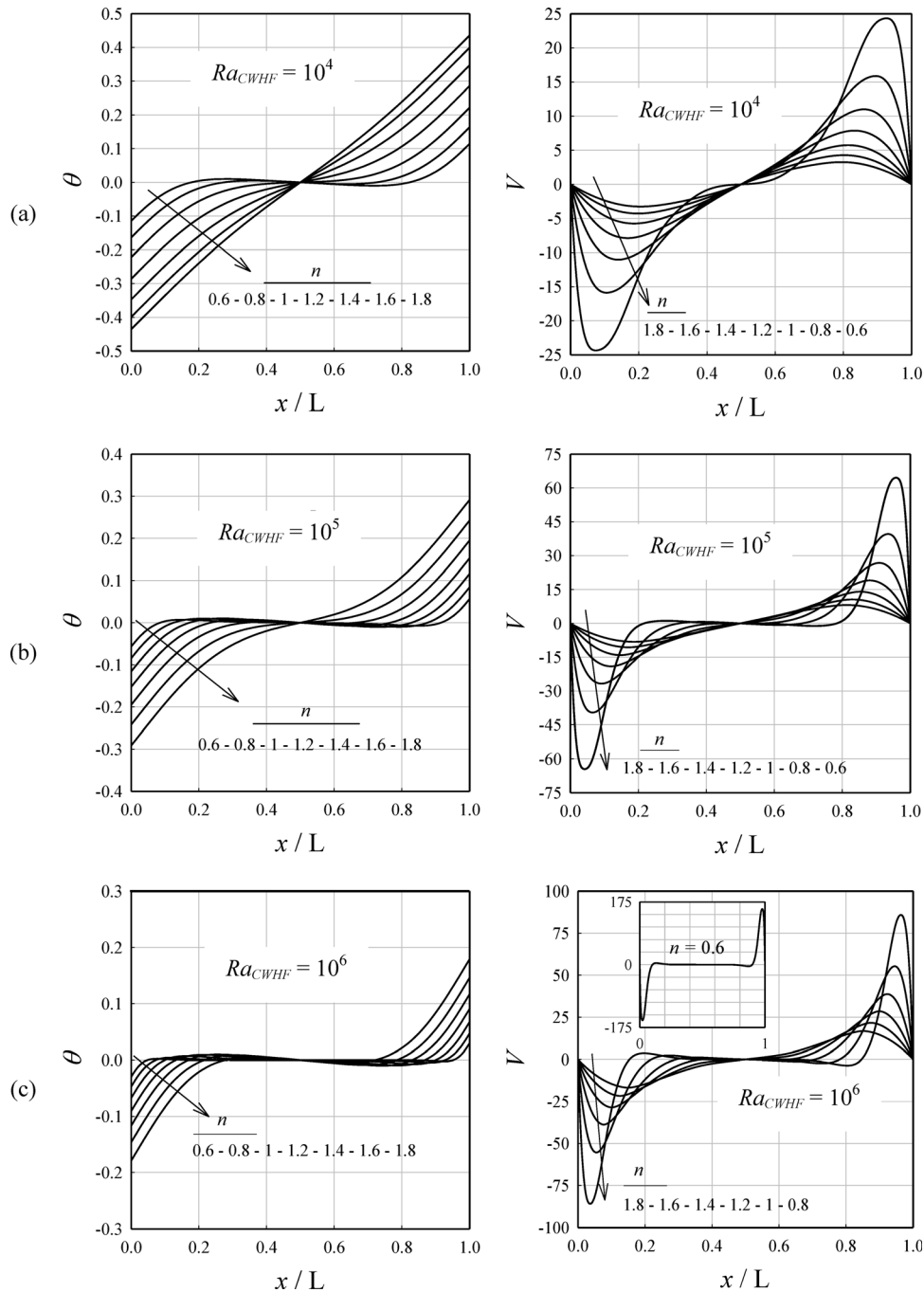


Fig. 3 Variations of nondimensional temperature θ and vertical velocity component V along the horizontal midplane at $Pr = 100$: (a) $Ra_{CWHF} = 10^4$, (b) $Ra_{CWHF} = 10^5$, and (c) $Ra_{CWHF} = 10^6$

indicates that the effects of convection strengthen with decreasing values of n . Figure 3 also demonstrates that the magnitude of vertical velocity component V increases significantly with decreasing n for fixed Ra_{CWHF} . The increasing magnitude of V indicates strengthening of convective transport with decreasing n which in turn leads to an increasing boundary layer character of temperature distribution. Equation (24) shows that the effective Grashof number $Gr_{CWHF,eff}$ increases significantly with decreasing values of n for a given value of Gr_{CWHF} , which indicates that the buoyancy force becomes increasingly strong in comparison to viscous force with decreasing values of n . This effect is particularly strong for fluids with $n < 1$ as a consequence of shear thinning. In con-

trast, the effects of buoyancy force become increasingly weak in comparison to viscous force with increasing n especially in fluids with $n > 1$ because of shear thickening. The $Ra_{CWHF} = 10^4$ and $n = 1.8$ data show that the heat transfer takes place principally due to thermal conduction as the convection strength is very weak. This predominant conduction-driven transport is reflected in the almost linear distribution of θ with x_1/L and negligible magnitude of V for this case. The conduction dominated thermal transport for $Ra_{CWHF} = 10^4$ and $n = 1.8$ is expected according to the scaling estimates given by Eq. (20), which indicates that δ_{th} becomes of the order of L for large values of n , indicating conduction-driven thermal transport.

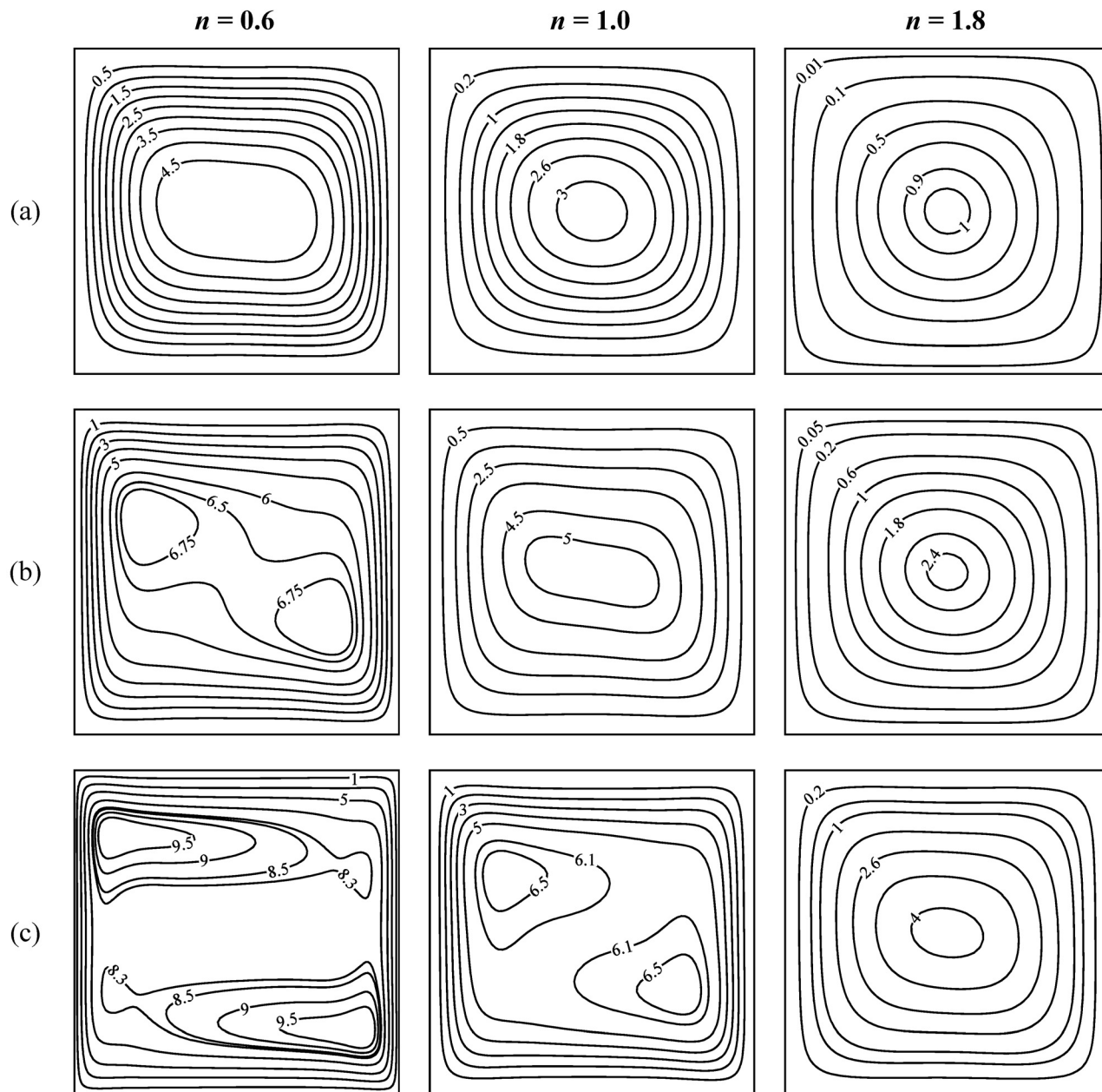


Fig. 4 Contours of nondimensional stream functions ($\Psi = \psi/\alpha$) for $n = 0.6, 1.0,$ and 1.8 at $Pr = 1000$: (a) $Ra_{CWHF} = 10^4$, (b) $Ra_{CWHF} = 10^5$, and (c) $Ra_{CWHF} = 10^6$

The contours of dimensionless stream function $\Psi = \psi/\alpha$ and dimensionless temperature $\theta = (T - T_{cen})k/qL$ for $Ra_{CWHF} = 10^4, 10^5,$ and 10^6 at $Pr = 10^3$ are shown in Figs. 4 and 5, respectively. It is evident from Fig. 4 that the magnitude of Ψ decreases (increases) with increasing (decreasing) n because of weakening (strengthening) of convective transport in comparison to viscous flow resistance. Moreover, it can be seen from Fig. 5 that the contours of dimensionless temperature becomes progressively more curved with decreasing n as a result of the strengthening of convective transport. Figure 5 further shows that the thermal boundary-layer thickness (δ_{th}) increases with increasing n , which is consistent with the scaling estimations given by Eq. (20), which predicts an increase in δ_{th} with increasing n for a given set of values of Ra_{CWHF} and Pr . It is also worth noting from Fig. 5 that the

temperature values along the vertical walls are not constant as expected in the case of CWHF boundary condition.

A decrease in the thermal boundary-layer thickness δ_{th} gives rise to a decrease in the magnitude of temperature difference between the vertical walls $\Delta T \sim q\delta_{th}/k$ (see Eq. (13)), which acts to enhance the mean Nusselt number $\overline{Nu} \sim qL/\Delta Tk \sim L/\delta_{th}$ (see Eq. (14)) for the CWHF configuration as can be seen in Fig. 6 where the variations of mean Nusselt number \overline{Nu} with Ra_{CWHF} are shown for different values of n at $Pr = 10^2, 10^3,$ and 10^4 . The results shown in Fig. 6 are consistent with the scaling estimate given by Eq. (21), which suggests that \overline{Nu} increases with decreasing n for a given set of values of Ra_{CWHF} and Pr . This behavior is also qualitatively consistent with the findings of Lamsaadi et al. [15,16] for the same configuration. Moreover, the increase

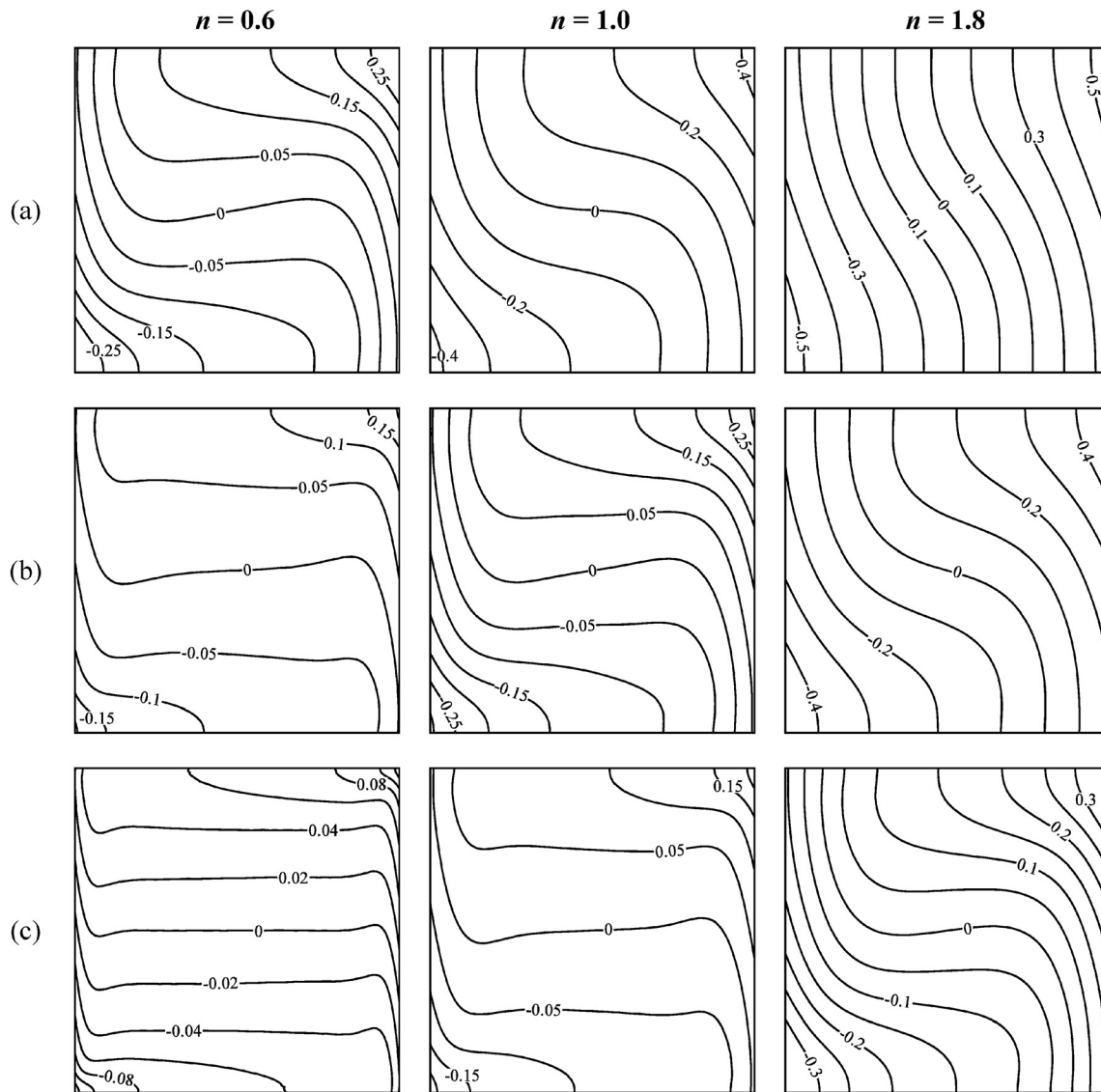


Fig. 5 Contours of nondimensional temperature θ for $n=0.6$, 1.0 , and 1.8 at $Pr=1000$: (a) $Ra_{CWHF} = 10^4$, (b) $Ra_{CWHF} = 10^5$, and (c) $Ra_{CWHF} = 10^6$

(decrease) in \overline{Nu} with decreasing (increasing) n is qualitatively similar to the earlier findings in the CWT configuration [14,23].

4.2 Effects of Nominal Rayleigh Number. It is useful to investigate the distributions of dimensionless temperature θ and the velocity components V (see Fig. 3) in order to understand the effects of Ra_{CWHF} on the heat transfer rate during natural convection of power-law fluids in a square enclosure. As seen from Fig. 3, the distribution of θ shows increasing boundary layer character with increasing Ra_{CWHF} for a given value of n . The linear (nonlinear) distribution of temperature with x_1 direction is indicative of conduction (convection) dominated thermal transport. An increase in Ra_{CWHF} gives rise to strengthening of buoyancy forces in comparison to viscous forces. It can also be observed from the distribution of V in Fig. 3 that the magnitude of V increases with increasing Ra_{CWHF} . This enhancement of fluid velocity magnitude is consistent with the fact that $Gr_{CWHF,eff}$ and $Ra_{CWHF,eff}$ increase with increasing Ra_{CWHF} for a given set of values of n and Pr (see Eqs. (24) and (25)).

Figures 4 and 5 also indicate that the effects of convection strengthen with increasing Ra_{CWHF} that is reflected in the augmentation in the magnitude of Ψ and progressively curved contours of dimensionless temperature for higher values of Ra . It is clear from Figs. 3 and 5 that δ_{th} decreases with increasing Ra_{CWHF} (for a given set of values of n and Pr), which is consistent with the scaling estimates given by Eq. (20). The thinning of δ_{th} for larger values of Ra acts to decrease the magnitude of temperature difference $\Delta T \sim q\delta_{th}/k$ between the vertical walls (as Eq. (13) and (14) indicate), which gives rise to an increase in $\overline{Nu} \sim qL/\Delta Tk$. The increase in \overline{Nu} with increasing Ra_{CWHF} is demonstrated in Fig. 6, which is also consistent with the scaling estimate given by Eq. (21). The Ra dependence of \overline{Nu} for different values of n is found to be qualitatively consistent with the earlier results by Lamsaadi et al. [15,16] in the CWHF configuration and the previous findings [14,23] in the CWT configuration.

4.3 Comparison Between the Constant Wall Heat Flux and Constant Wall Temperature Cases. For the purpose of a quantitative comparison between CWHF and CWT cases, it is

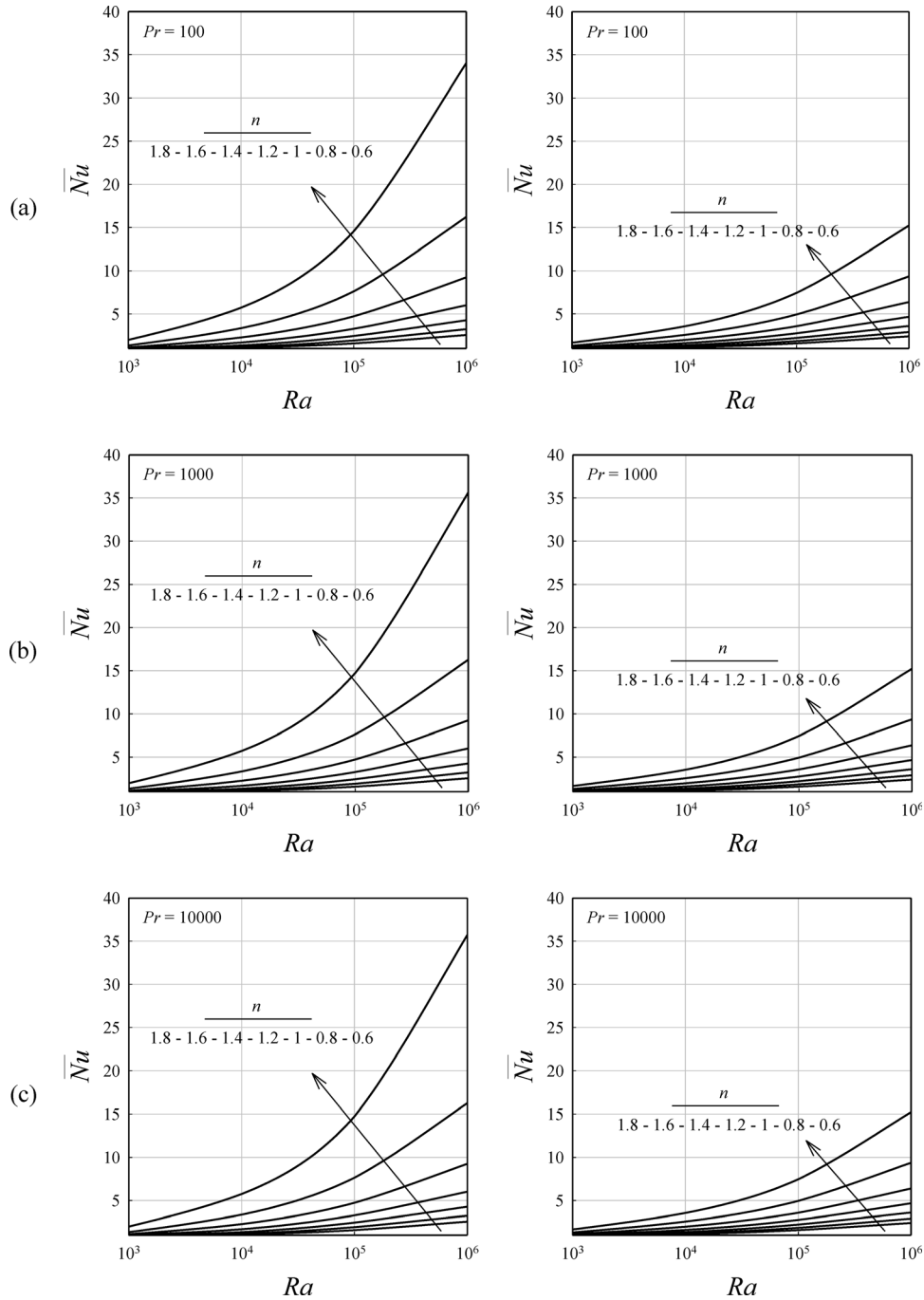


Fig. 6 The variation of the mean Nusselt number with Rayleigh number for both CWT (left column) and CWHF (right column) configurations for different values of power-law index n at (a) $Pr = 100$, (b) $Pr = 1000$, and (c) $Pr = 10,000$

useful to refer to the definitions of nominal Ra_{CWT} and Gr_{CWT} for the CWT configuration [23], which were provided in Eq. (10ii). The balance between inertial and buoyancy forces according to Eq. (17) leads to an expression for the characteristic velocity scale for the CWT configuration [23]

$$v \sim \sqrt{g\beta\Delta TL} \quad (31)$$

Using this expression in Eq. (16) the thermal boundary-layer thickness for the CWT configuration can be estimated as [23]

$$\begin{aligned} \delta_{th} &\sim \min \left[L, \frac{1}{f_4(Ra_{CWT}, Pr, n)} \left(\frac{KL(g\beta\Delta TL)^{n/2-1}}{\rho} \right)^{\frac{1}{n+1}} \right] \\ &\sim \min \left[L, \frac{1}{f_4(Ra_{CWT}, Pr, n)} \frac{L}{(Ra_{CWT}^{2-n} Pr^{-n})^{\frac{1}{2(n+1)}}} \right] \end{aligned} \quad (32)$$

Equation (32) shows that the thermal boundary-layer δ_{th} decreases (increases) with decreasing (increasing) n . Substitution of Eq. 32 into Eq. 13 yields

$$\overline{Nu} \sim (Ra_{CWT} Pr^{-n})^{\frac{1}{2(n+1)}} f_4(Ra_{CWT}, Pr, n) \quad \text{when } \overline{Nu} > 1 \quad (33)$$

The variation of \overline{Nu} with the same numerical values of Ra_{CWT} and Ra_{CWHF} for both CWT and CWHF configuration for different values of n are shown in Fig. 6 for a given set of values of Pr . It is evident from Fig. 6 that \overline{Nu} increases with increasing values of Ra_{CWHF} (Ra_{CWT}) for both configurations, which is also consistent with scaling estimates given by Eqs. (21) and (33). Besides, it is also apparent from Fig. 6 that the values of \overline{Nu} for the CWT and CWHF configurations are comparable for the same values of Ra_{CWHF} and Ra_{CWT} when Ra remains small. However, the difference between the values of \overline{Nu} increases with increasing Ra_{CWHF} (Ra_{CWT}). For a given value of Pr , the mean Nusselt number for the CWT case scales as $\overline{Nu} \sim (Ra_{CWT})^{\frac{1}{2(n+1)}}$, whereas it scales as $\overline{Nu} \sim (Ra_{CWHF})^{\frac{1-n}{2(n+2)}}$ for the CWHF case. The difference between the two Ra exponents ($\frac{1}{2(n+1)}$ and $\frac{1-n}{2(n+2)}$) increases with increasing Ra and this gives rise to an increase in the difference between the \overline{Nu} values in the two configurations with increasing Ra_{CWHF} (Ra_{CWT}) and this effect is especially prevalent for shear-thinning fluids ($n < 1$) (see Fig. 6). The difference between the \overline{Nu} values for the CWT and CWHF configurations with increasing Ra_{CWHF} (Ra_{CWT}) becomes more noticeable with decreasing n , which is also in agreement with the scaling arguments (see Eqs. (21) and (33)).

The difference between the \overline{Nu} values for the CWHF and CWT configurations can be explained using the differences in the distributions of θ and V for both the configurations that are presented in Figs. 7 and 8, respectively. For the CWT case the nondimensional temperature θ is defined as $\theta = (T - T_{cen}) / (T_H - T_C)$, where T_{cen} is the temperature at the geometric center of the domain. Under predominantly conduction-driven thermal transport the temperature difference between the vertical walls remain equal to $qL/k = (T_H - T_C)$. The temperature difference between the vertical sidewalls in the CWHF condition at very small values of Ra_{CWHF} , where the thermal transport is primarily conduction-driven, remains identical to the temperature difference between the vertical sidewall under the CWT condition for the same numerical value of Ra_{CWT} . As the value of Ra_{CWHF} increases, the temperature difference decreases in comparison to qL/k in the CWHF configuration, whereas it remains exactly equal to $(T_H - T_C)$ for all values of Ra_{CWT} in the CWT configuration. As the temperature difference between the vertical sidewall is smaller in the CWHF configuration than in the CWT configuration, the velocity induced in the enclosure is smaller in magnitude in the CWHF configuration than in the CWT configuration for the same numerical values of Ra_{CWHF} and Ra_{CWT} (see Fig. 8). The smaller values of velocity magnitude in the CWHF configuration than in the CWT configuration for the same numerical values of Ra_{CWHF} and Ra_{CWT} are reflected in the smaller value of \overline{Nu} in the CWHF configuration than in the CWT configuration in the convection-dominated thermal transport regimes.

4.4 Correlation for Mean Nusselt Number \overline{Nu} . Based on the scaling relation given by Eq. (33), Turan et al. [23] proposed a correlation for \overline{Nu} for square enclosure with CWT condition for $Ra_{CWT} = 10^4 - 10^6$ and $Pr = 10^2 - 10^4$ in the following manner:

$$\overline{Nu} = 0.162 Ra_{CWT}^{0.043} \frac{Pr^{0.341}}{(1 + Pr)^{0.091}} \left(\frac{Ra_{CWT}}{Pr^n} \right)^{\frac{1}{2(n+1)}} e^{b(n-1)} \quad (34i)$$

where b is a correlation parameter expressed as

$$b = 1.343 Ra_{CWT}^{0.065} Pr^{0.036} \quad \text{for } n \leq 1 \quad (34ii)$$

$$b = 0.858 Ra_{CWT}^{0.071} Pr^{0.034} \quad \text{for } n > 1 \quad (34iii)$$

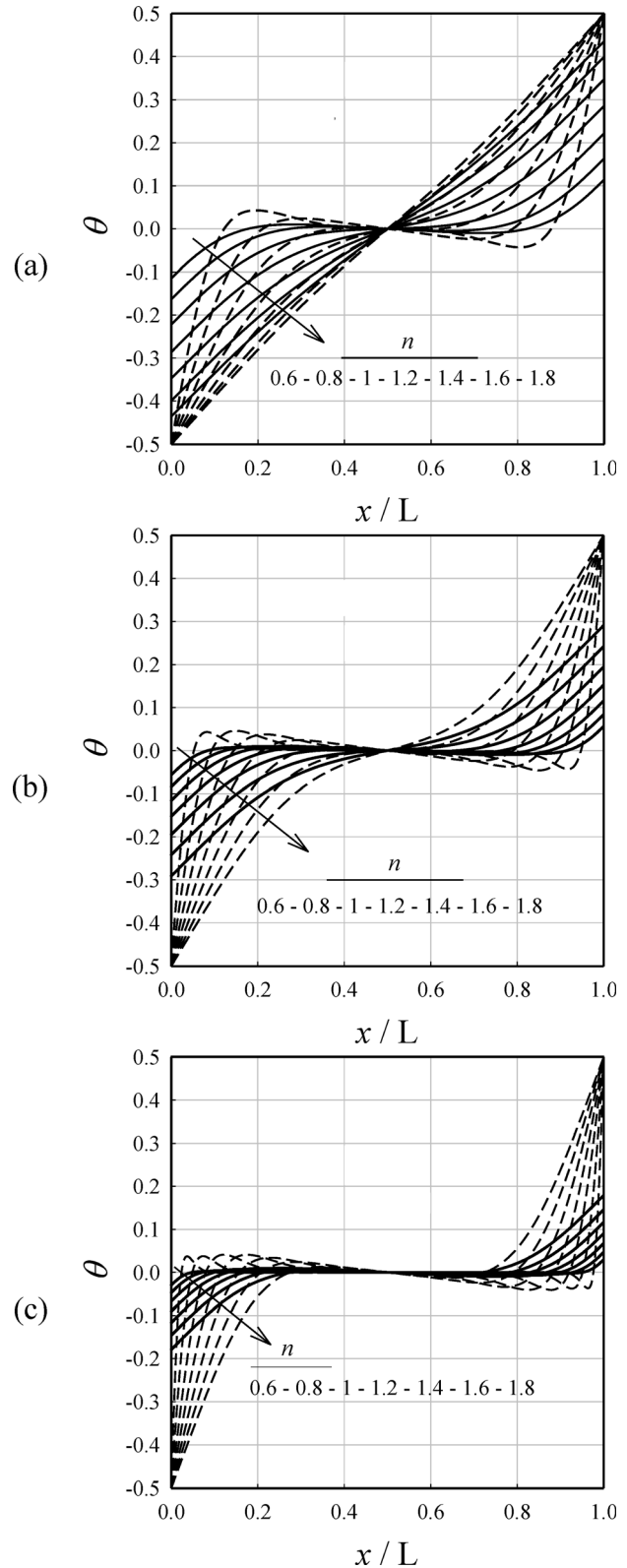


Fig. 7 Variations of nondimensional temperature θ along the horizontal midplane for both (- - -) CWT, (—) CWHF configurations at different values of n for the same values of Ra_{CWHF} and Ra_{CWT} : $Ra_{CWHF} = Ra_{CWT}$: (a) 10^4 , (b) 10^5 , and (c) 10^6 at $Pr = 1000$

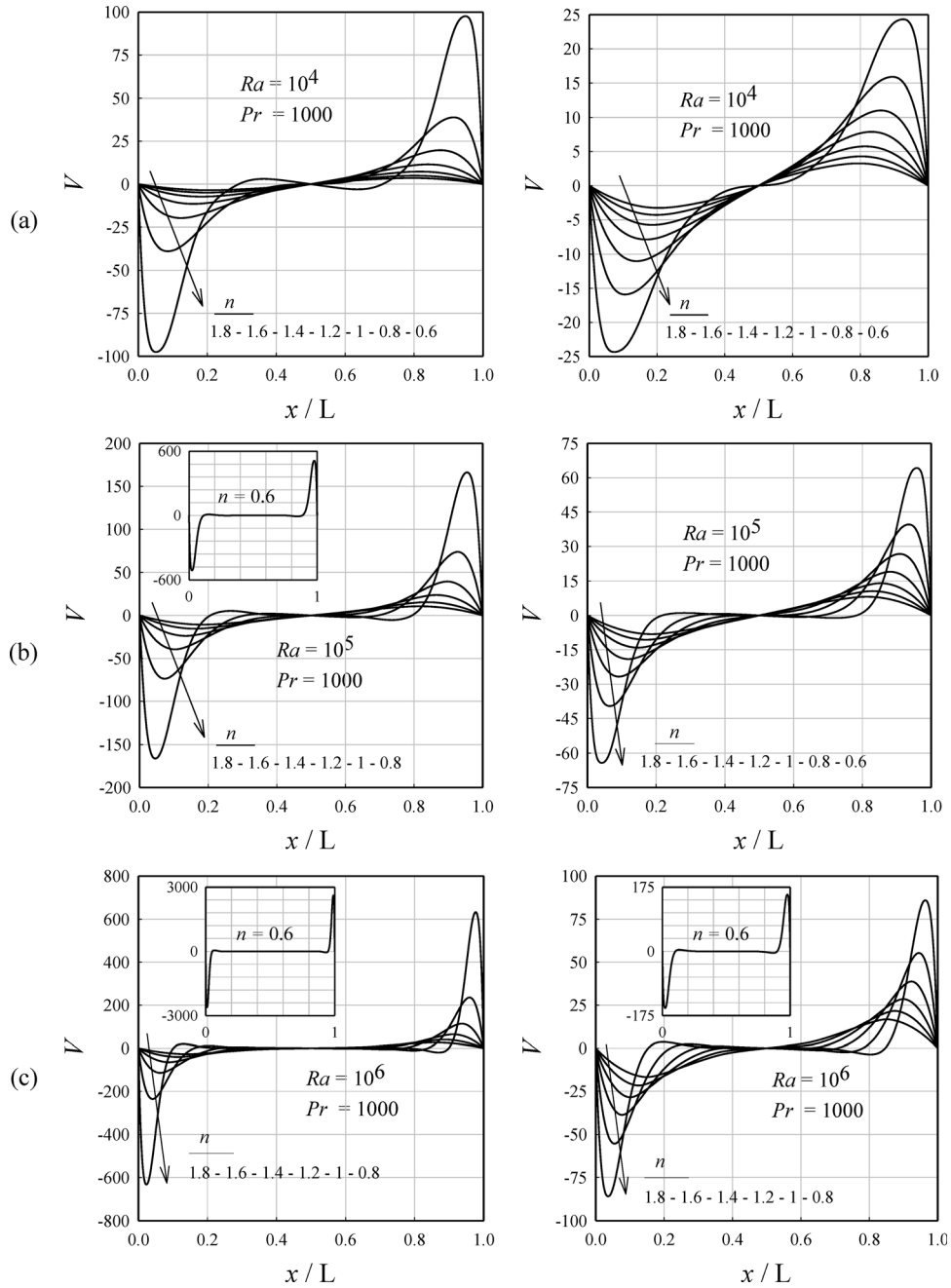


Fig. 8 Variations of nondimensional vertical velocity V along the horizontal midplane for both CWT (left column), CWHF (right column) configurations at different values of n for the same values of Ra_{CWHF} and Ra_{CWT} : $Ra_{CWHF} = Ra_{CWT} = (a) 10^4$, $(b) 10^5$, and $(c) 10^6$ at $Pr = 1000$

The correlation for CWT given by Eqs. (34i)–(34iii) is modified here in order to propose a correlation for the CWHF case. According to Eq. (21) the mean Nusselt number \overline{Nu} can be taken to scale with $\overline{Nu} \sim \left(Ra_{CWHF} Pr^{-n/2} \right)^{[1/(n/(2+2))]} f_3(Ra_{CWHF}, Pr, n)$ and recently Turan et al. [22] demonstrated that $\overline{Nu} = 0.209 Ra_{CWHF}^{0.249} [Pr/(1+Pr)]^{0.031}$ satisfactorily captures the Ra_{CWHF} and Pr dependences of \overline{Nu} for Newtonian fluids, and thus, the correlation for \overline{Nu} for power-law fluids should be proposed in such a manner that $\lim_{n \rightarrow 1} \overline{Nu} = 0.209 Ra_{CWHF}^{0.249} [Pr/(1+Pr)]^{0.031}$. Based on the aforementioned observations and limiting conditions, a correlation for \overline{Nu} is proposed here in the following manner:

$$\overline{Nu} = 0.209 Ra_{CWHF}^{0.049} \frac{Pr^{0.231}}{(1+Pr)^{0.031}} \left(\frac{Ra_{CWHF}^{1-n/2}}{Pr^{n/2}} \right)^{\frac{1}{n/2+2}} e^{b_1(n-1)} \quad (35i)$$

where b_1 is a correlation parameter which can be expressed based on simulation results as

$$b_1 = c_1 Ra_{CWHF}^{c_2} Pr^{c_3} \quad (35ii)$$

where c_1 , c_2 , and c_3 are given by

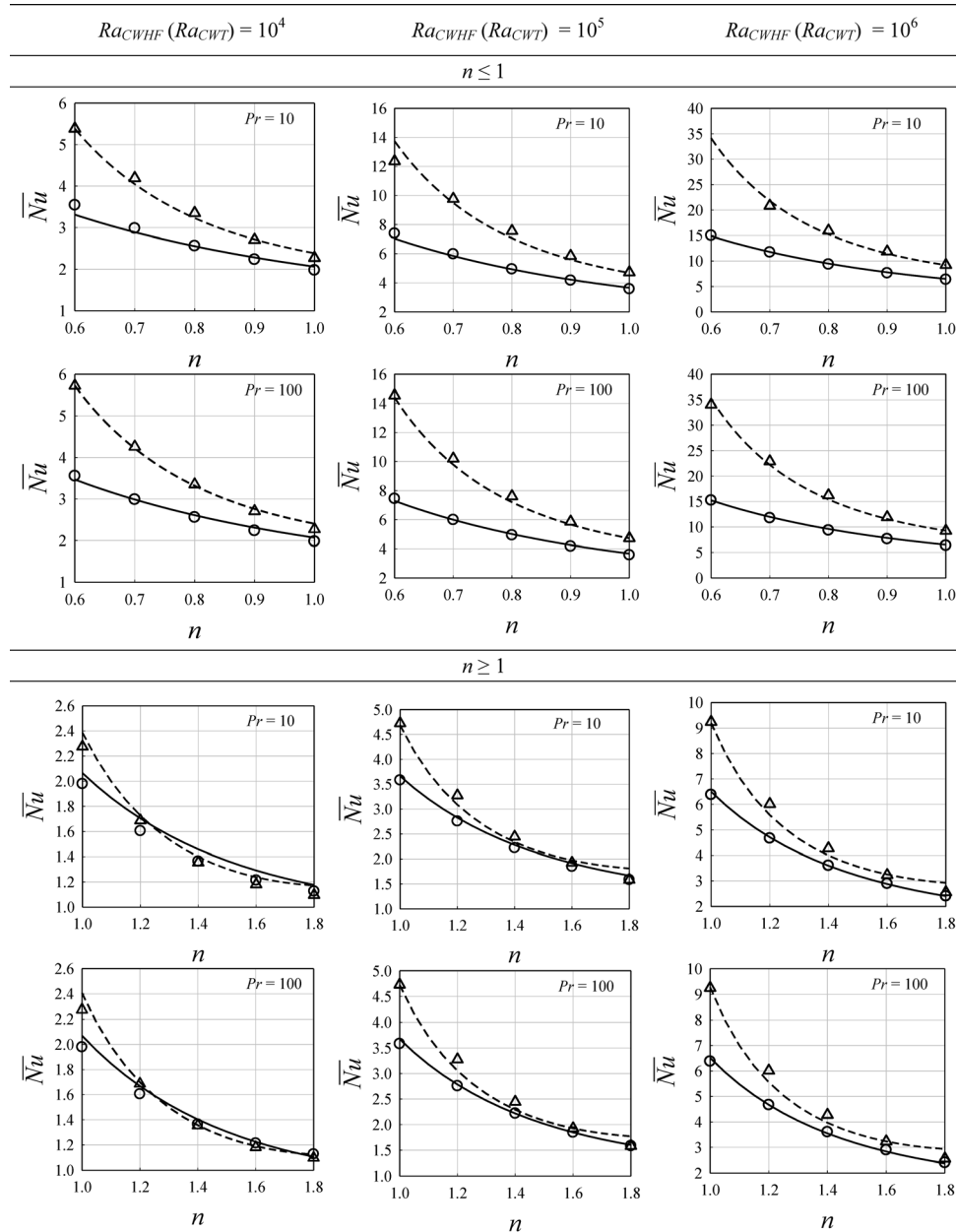


Fig. 9 Variations of \overline{Nu} with power-law index for both CWT (Δ) and CWHF (\circ) configurations for different values of Pr and Ra_{CWT} (Ra_{CWHF}) along with the predictions of Eqs. (34i)–(34iii) (---) and Eqs. (35i)–(35iv) (—)

$$c_1 = 0.965; \quad c_2 = 0.038; \quad \text{and} \quad c_3 = 0.072 \quad \text{for} \quad n \leq 1 \quad (35iii)$$

$$c_1 = 0.815; \quad c_2 = 0.052; \quad \text{and} \quad c_3 = 0.063 \quad \text{for} \quad n > 1 \quad (35iv)$$

According to Eqs. (35i)–(35iv) the expression for \overline{Nu} becomes exactly equal to an existing correlation for Newtonian fluids [22] when $n = 1$. The performance of the correlations given by Eqs. (35i)–(35iv) (Eqs. (34i)–(34iii)) for fluids with $n \leq 1$ and $n > 1$ for $Ra_{CWHF}(Ra_{CWT}) = 10^4 - 10^6$ and $Pr = 10 - 10^2$ are shown in Fig. 9. It can be seen from Fig. 9 that the correlation given by Eqs. (35i)–(35iv) (Eqs. (34i)–(34iii)) predicts \overline{Nu} satisfactorily for the CWHF (CWT) configuration in the range of nominal Ra and Pr numbers considered here.

5 Conclusions

Laminar natural convection of power-law non-Newtonian fluids in a square enclosure with vertical sidewalls subjected to CWHF boundary condition has been numerically studied for power-law index n in the range 0.6–1.8, for $Ra_{CWHF} = 10^4 - 10^6$ and $Pr = 10 - 10^5$. The effects of n , Ra_{CWHF} , and Pr on heat and momentum transport have been systematically investigated and the results have been compared with the corresponding results obtained from the CWT boundary condition. It has been found that the mean Nusselt number \overline{Nu} increases with increasing values of Ra for both Newtonian and power-law fluids. The Nusselt number was found to decrease with increasing power-law index n , and, for large values of n , the value of mean Nusselt number settled to unity (i.e., $\overline{Nu} = 1$) as the heat transfer took place

principally by conduction for both CWT and CWHF boundary conditions. It was also shown that \overline{Nu} for both the CWHF and CWT configurations remains comparable for the same numerical value of Ra_{CWHF} and Ra_{CWT} for small values of nominal Ra and large values of n . However, the difference between the \overline{Nu} values obtained for CWT and CWHF boundary conditions for the same numerical values of Ra_{CWHF} and Ra_{CWT} increases with increasing Ra and decreasing n . The simulation results show that the mean Nusselt number \overline{Nu} is virtually unaffected by the increase in Pr (at least in the range $Pr = 10-10^5$) for Newtonian and power-law fluids for a given set of values of Ra_{CWHF} (Ra_{CWT}) and power-law index n . Finally, guided by a scaling analysis, the simulation results are used to propose a new correlation for \overline{Nu} for power-law fluids with n ranging from 0.6 to 1.8. This correlation is shown to satisfactorily capture the variation of \overline{Nu} with Ra_{CWHF} (Ra_{CWT}), Pr , and n for all the cases considered in this study. Moreover, this correlation reduces to an existing correlation for \overline{Nu} for Newtonian fluids when $n = 1$.

It is worth noting that the temperature dependences of thermophysical properties such as consistency and thermal conductivity have been neglected in the present analysis as a first step to aid the fundamental understanding of natural convection in power-law fluids following several previous studies [14–16,23,24]. Although the inclusion of temperature-dependent thermophysical properties are not expected to change the qualitative behavior observed in the present study, as the convection pattern is found to be qualitatively similar for all values of n , Ra , and Pr within the laminar steady convection regime. However, the inclusion of temperature dependence of consistency K , power-law index n and thermal conductivity k is probably necessary for quantitative predictions. Thus, future investigation on the same configuration with temperature-dependent thermophysical properties of power-law fluids will be necessary for deeper understanding and more accurate quantitative predictions.

Nomenclature

c_p	= specific heat at constant pressure (J/kgK)
e	= relative error
e_{ij}	= rate of strain tensor (s^{-1})
g	= gravitational acceleration (m/s^2)
Gr	= Grashof number
Gr_{CWT}	= Grashof number for constant wall temperature configuration
Gr_{CWHF}	= Grashof number for constant wall heat flux configuration
h	= heat transfer coefficient (W/m^2K)
K	= consistency ($N \cdot s^n/m^2$)
k	= thermal conductivity (W/mK)
L	= Length and height of the enclosure (m)
n	= power-law index
Pr	= Prandtl number
\overline{Pr}_{CWT}	= Prandtl number for constant wall temperature configuration
\overline{Pr}_{CWHF}	= Prandtl number for constant wall heat flux configuration
q	= heat flux (W/m^2)
Ra	= Rayleigh number
Ra_{CWT}	= Rayleigh number for constant wall temperature configuration
Ra_{CWHF}	= Rayleigh number for constant wall heat flux configuration
T	= temperature (K)
t	= time(s)
u_i	= i^{th} velocity component (m/s)
U, V	= dimensionless horizontal ($U = u_1 L/\alpha$) and vertical velocity ($V = u_2 L/\alpha$)
ϑ	= characteristic velocity (m/s)
x_i	= coordinate in i^{th} direction (m)
α	= thermal diffusivity (m^2/s)

β	= coefficient of thermal expansion (1/K)
δ, δ_{th}	= velocity and thermal boundary-layer thickness (m)
θ	= dimensionless temperature, ($\theta = (T - T_{cen}) / (T_H - T_C)$)
μ	= dynamic viscosity (Ns/m^2)
ν	= kinematic viscosity (m^2/s)
ρ	= density (kg/m^3)
τ_{ij} (τ)	= stress tensor (stress) (Pa)
ϕ	= general primitive variable
ψ	= stream function (m^2/s)
Ψ	= dimensionless stream function ($\Psi = \psi/\alpha$)

Subscripts

a	= apparent
C	= cold wall
cen	= geometric center of the domain
CWHF	= constant wall heat flux
CWT	= constant wall temperature
eff	= effective value
ext	= extrapolated value
H	= hot wall
max	= maximum value
ref	= reference value
wall	= wall value

Special Character

ΔT	= difference between hot and cold wall temperature ($= (T_H - T_C)$) (K)
------------	---

References

- [1] de Vahl Davis, G., 1983, "Natural Convection of Air in a Square Cavity: A Bench Mark Numerical Solution," *Int. J. Numer. Meth. Fluids*, **3**, pp. 249–264.
- [2] Emery, A. F., and Lee, J. W., 1999, "The Effects of Property Variations on Natural Convection in a Square Enclosure," *ASME J. Heat Transfer*, **121**, pp. 57–62.
- [3] Aydin, O., Ünal, A., and Ayhan, T., 1999, "Natural Convection in Rectangular Enclosures Heated From One Side and Cooled From Above," *Int. J. Heat Mass Transf.*, **42**, pp. 2345–2355.
- [4] Ostrach, S., 1988, "Natural Convection in Enclosures," *ASME J. Heat Transfer*, **110**, pp. 1175–1190.
- [5] Bejan, A., 1984, *Convection Heat Transfer*, John Wiley Sons Inc., New York.
- [6] Ozoë, H., and Churchill, S. W., 1972, "Hydrodynamic Stability and Natural Convection in Ostwald–De Waele and Ellis Fluids: The Development of a Numerical Solution," *AIChE J.*, **18**, pp. 1196–1207.
- [7] Lamsaadi, M., Naïmi, M., and Hasnaoui, M., 2005, "Natural Convection of Non-Newtonian Power Law Fluids in a Shallow Horizontal Rectangular Cavity Uniformly Heated From Below," *Heat Mass Transf.*, **41**, pp. 239–249.
- [8] Ohta, M., Ohta, M., Akiyoshi, M., and Obata, E., 2002, "A Numerical Study on Natural Convective Heat Transfer of Pseudoplastic Fluids in a Square Cavity," *Numer. Heat Transf. A*, **41**, pp. 357–372.
- [9] Inaba, H., Dai, C., and Horibe, A., 2003, "Natural Convection Heat Transfer of Microemulsion Phase-Change-Material Slurry in Rectangular Cavities Heated From Below and Cooled From Above," *Int. J. Heat Mass Transf.*, **46**, pp. 4427–4438.
- [10] Zhang, J., Vola, D., and Frigaard, I. A., 2006, "Yield Stress Effects on Rayleigh–Bénard Convection," *J. Fluid Mech.*, **566**, pp. 389–419.
- [11] Balmforth, N. J., and Rust, A. C., 2009, "Weakly Nonlinear Viscoplastic Convection," *J. Non-Newton. Fluid Mech.*, **158**, pp. 36–45.
- [12] Vikhansky, A., 2009, "Thermal Convection of a Viscoplastic Liquid with High Rayleigh and Bingham Numbers," *Phys. Fluids*, **21**, p. 103103.
- [13] Park, H. M., and Ryu, D. H., 2001, "Rayleigh–Bénard Convection of Viscoplastic Fluids in Finite Domains," *J. Non-Newton. Fluid Mech.*, **98**, pp. 169–184.
- [14] Kim, G. B., Hyun, J. M., and Kwak, H. S., 2003, "Transient Buoyant Convection of a Power Law Non-Newtonian Fluid in an Enclosure," *Int. J. Heat Mass Transf.*, **46**, pp. 3605–3617.
- [15] Lamsaadi, M., Naïmi, M., Hasnaoui, M., and Mamou, M., 2006, "Natural Convection in a Vertical Rectangular Cavity Filled With a Non-Newtonian Power Law Fluid and Subjected to a Horizontal Temperature Gradient," *Numer. Heat Transf. Part A*, **49**, pp. 969–990.
- [16] Lamsaadi, M., Naïmi, M., and Hasnaoui, M., 2006, "Natural Convection Heat Transfer in Shallow Horizontal Rectangular Enclosures Uniformly Heated From the Side and Filled With Non-Newtonian Power Law Fluids," *Energy Convers. Manage.*, **47**, pp. 2535–2551.
- [17] Barth, W. L., and Carey, G. F., 2006, "On a Natural-Convection Benchmark Problem in Non-Newtonian Fluids," *Numer. Heat Transf. Part B*, **50**, pp. 193–216.

- [18] Leung, W. H., Hollands, K. G. T., and Brunger, A. P., 1998, "On a Physically Realizable Benchmark Problem in Internal Natural Convection," *Int. J. Heat Mass Transf.*, **41**, pp. 3817–3828.
- [19] Vola, D., Boscardin, L., and Latché, J. C., 2003, "Laminar Unsteady Flows of Bingham Fluids: A Numerical Strategy and Some Benchmark Results," *J. Comput. Phys.*, **187**, pp. 441–456.
- [20] Turan, O., Chakraborty, N., and Poole, R. J., 2010, "Laminar Natural Convection of Bingham Fluids in a Square Enclosure With Differentially Heated Side Walls," *J. Non-Newton. Fluid Mech.*, **165**, pp. 903–913.
- [21] Turan, O., Poole, R. J., and Chakraborty, N., 2011, "Aspect Ratio Effects in Laminar Natural Convection of Bingham Fluids in Rectangular Enclosures With Differentially Heated Side Walls," *J. Non-Newton. Fluid Mech.*, **166**, pp. 208–230.
- [22] Turan, O., Sachdeva, A., Poole, R. J., and Chakraborty, N., 2011, "Laminar Natural Convection of Bingham Fluids in a Square Enclosure With Vertical Walls Subjected to Constant Heat Flux," *Numer. Heat Transf. A*, **60**(5), pp. 381–409.
- [23] Turan, O., Sachdeva, A., Chakraborty, N., and Poole, R. J., 2011, "Laminar Natural Convection of Power-Law Fluids in a Square Enclosure With Differentially Heated Side Walls Subjected to Constant Temperatures," *J. Non-Newton. Fluid Mech.*, **166**, pp. 1049–1063.
- [24] Ng, M. L., and Hartnett, J. P., 1986, "Natural Convection in Power Law Fluids," *Int. Comm. Heat Mass Transf.*, **13**, pp. 115–120.
- [25] Patankar, S. V., 1980, *Numerical Heat Transfer and Fluid Flow*, Hemisphere, Washington, D.C.